Application of AMSR-E and AMSR2 Low-frequency Channel Brightness Temperature Data for Hurricane Wind Retrievals

Mingrun Mai[1], Biao Zhang[1, 2*], Xiaofeng Li[3], Paul A. Hwang[4], and Jun A. Zhang[5]

[1]School of Marine Sciences, Nanjing University of Information Science and Technology, Nanjing, Jiangsu, China.

[2]Jiangsu Research Center for Ocean Survey and Technology, Nanjing, Jiangsu, China

[3]GST at NOAA/NEDIS, College Park, Maryland, USA.

[4]Remote Sensing Division, Naval Research Laboratory, Washington, DC, USA.

[5]Hurricane Research Division at NOAA/AOML and CIMAS at University of Miami, Miami, Florida, USA.

Submitted to IEEE Transactions on Geoscience and Remote Sensing
January, 2016
Revised

Corresponding Author
Dr. Biao Zhang
School of Marine Sciences
Nanjing University of Information Science and Technology
219 Ningliu Road, Nanjing, Jiangsu, 210044 CHINA
Email: zhangbiao@nuist.edu.cn

Abstract

We present a method to retrieve wind speeds in hurricanes from spaceborne passive microwave radiometer data. The AMSR-E and AMSR2 onboard Earth Observing System (EOS) Aqua and Global Change Observation Mission-Water 1 (GCOM-W1) satellites brightness temperature (T_B) observations acquired at 6.9 GHz horizontal polarization channel are selected for wind retrieval due to the fact that the signal at this frequency is sensitive to high wind speeds, but less sensitive to rain scatter than those acquired at other higher frequency channels. The AMSR-E and AMSR2 observations of 53 hurricanes between 2002 and 2014 are collected and collocated with Stepped-Frequency Microwave Radiometer (SFMR) measurements. Based on the small slope approximation (SSA)/small perturbation method (SPM) model, and an ocean surface roughness spectrum, the wind speeds are retrieved from the T_B data and validated against the SFMR measurements. Statistical comparison of the entire dataset shows that the bias and root-mean-square error (RMSE) of the retrieved wind speeds are 1.11 and 4.34 m/s, respectively, which suggests that the proposed method can obtain high wind speeds under hurricane conditions. Two case studies show that the wind speed retrieval bias and RMSE are 1.08 and 3.93 m/s for Hurricane Earl, and 0.09 and 3.23 m/s for Hurricane Edouard, respectively. The retrieved wind speeds from the AMSR-E and AMSR2 continuous three-day observations clearly show the process of hurricane intensification and weakening.

1. Introduction

The wind passing over the ocean drives a full range of ocean circulations and waves, and also modulates the air-sea exchanges of heat, moisture, and gases. Wind speed is a fundamental parameter that needs accurate global measurements for the purpose of running operational weather models and providing warnings for shipping and fishery vessels when storms approach. Buoys and ships can routinely provide *in situ* surface wind speed measurements in specific and sparse geographical locations only. However, the anemometers onboard buoys and ships lose their functionality under extreme weather events such as tropical cyclones.

The active microwave scatterometers such as QuikSCAT and ASCAT onboard the SeaWinds and Metop-A satellites are able to monitor hurricane wind fields with large area coverage [1-4]. Synthetic aperture radars (SARs) have the capability to measure ocean surface winds under moderate sea state with systematic errors of less than 2 m/s [5-8]. Co-polarized (HH or VV) SAR measurements have been applied to retrieving high wind speeds [9-13], but the retrieval accuracy is affected by the radar backscattering saturation under hurricane or typhoon conditions. Studies show that cross-polarized (HV or VH) SAR returns may improve hurricane or typhoon surface wind retrieval, but signal insensitivity due to surface roughness and foam saturation may remain an issue for cross-polarization sea returns [14-21].

Spaceborne passive microwave radiometers are also very useful instruments for measuring ocean surface wind speeds. Statistical and physical-based methods have been widely used to retrieve wind speeds under moderate sea states via radiometer brightness temperature (T_B) observations. The statistical algorithm uses regression or an artificial neural network (ANN) technique to derive the relationship between the T_B and the ocean surface wind speed [22-23]. The physical-based algorithm employs a radiative transfer model (RTM) [24-25], which requires an accurate ocean surface microwave emissivity estimation, as well as atmospheric temperature and water vapor profiles. Both types of algorithms have been applied for high wind retrievals [25-28]. The T_B data acquired at 6.9 GHz (C-band), 10.7 GHz (X-band), or 1.4 GHz (L-band) have been used to retrieve high wind speeds, because the signals observed at these lower frequencies are sensitive to high wind speeds and less affected by rain and atmospheric effects than those at higher frequencies.

Previous studies have shown that raindrops have an important influence on the ocean surface microwave signal. For example, rain increases the atmospheric attenuation, particularly at higher radar frequencies [29], but the rain scattering can be ignored if the microwave wavelength is much larger than the raindrop size. The T_B acquired at 1.4 GHz is suitable for remote sensing of hurricane wind speeds [28], and raindrop-induced scattering can be neglected for frequencies below 10 GHz when the rain rate is less than 12 mm/h [22, 30]. The AMSR-E and AMSR2 provide measurements at these relatively lower frequency channels (6.9 GHz and 10.7 GHz). Recently, the AMSR2 T_B data acquired at 10.7 GHz channel have been applied to retrieve the ocean surface wind speeds of the polar low over the North Sea, which can reduce the masking area under severe marine conditions. [26]. It is noted that the effects of the atmospheric water vapor and cloud liquid water on the T_B at high latitudes are smaller than on those observed over the hurricanes in low and middle latitude regions. Moreover, the retrieval results [26] were only compared with the *in situ* surface wind speed measurements ranging from 4 to 26 m/s, and not validated using the high wind observations in hurricanes. Although the AMSR2 6.9 and 10.7 GHz T_B data have been further used to estimate the high wind speeds in extratropical cyclones, the proposed retrieval method is based on an ANN model [27].

In this study, an approach to retrieve high wind speeds in hurricanes using spaceborne microwave radiometer observations is proposed. This retrieval algorithm is based on a SSA/SPM model and a high sea state surface roughness spectrum (referred to as the H roughness spectrum hereafter). The ocean surface roughness which is driven by surface wind plays an important role in understanding the air-sea interaction, net momentum flux from air to ocean, wind wave generation, and changing ocean surface emissivity. An accurate interpretation of the active microwave radar backscatter, as well as the passive radiometer emission measurements, relies on a good understanding of the properties of ocean surface roughness. For example, a dimensionless surface roughness spectrum (H spectrum) has been empirically parameterized as a power-law function of the dimensionless wind speed, which is expressed as the ratio of the wind friction velocity and the phase speed of the surface roughness wave component [31]. This roughness spectrum can be applied to the computation of the normalized radar cross sections (NRCS) at low and moderate wind speeds. The H spectrum was further modified by incorporating wave spectra inverted from Ku-, C- and L-band GMFs over the wind speed ranging from mild to hurricane conditions to improve the active and passive microwave computations of the NRCS and brightness temperature in high winds [32].

The wind speed has a greater influence on the ocean surface emissivity at horizontal polarization than at vertical polarization [25]. In our proposed algorithm, the high wind speeds inside hurricanes are obtained by using the AMSR-E and AMSR2 T_B measurements at 6.9 GHz horizontal polarization channel. The proposed high wind speed retrieval algorithm is validated with the airborne SFMR along-track measurements in 53 hurricanes occurred between 2002 and 2014.

This paper is organized as follows: Section 2 describes the dataset used in this study; Section 3 illustrates the proposed high wind speed retrieval algorithm development; Section 4 presents the results and discussions; and Section 5 contains the summary.

2. Dataset

In this research, AMSR-E and AMSR2 T_B observations over hurricanes, SFMR along-track wind speed measurements and sea surface temperature (SST) used in the SFMR surface wind retrieval, and HYbrid Coordinate Ocean Model (HYCOM) model-simulated SST, are used to develop and validate a proposed high wind speed retrieval algorithm. These elements are described in the following subsections.

2.1 Spaceborne passive microwave radiometer observations

The AMSR-E is a six-frequency, twelve-channel conically scanning passive microwave radiometer onboard the Earth Observing System (EOS) Aqua satellite. It measures horizontally and vertically polarized T_B at 6.9, 10.7, 18.7, 23.8, 36.5, and 89 GHz. The mean spatial resolution and footprint size at 6.9 GHz are 56 km and 43 km by 75 km, respectively. At an altitude of 705 km, it measures the up-welling scene T_B over a swath of 1445 km.

The AMSR2 is onboard the Japan Aerospace Exploration Agency's (JAXA's) Global Change Observation Mission-Water 1 (GCOM-W1), and is also a conically scanning passive microwave radiometer that measures microwave emissions and scattering from the Earth's surface and atmosphere. The AMSR2 is similar to the AMSR-E. However, it adds extra horizontal and vertical polarization channels at 7.3 GHz, and its swath is 1450 km. The addition of the two new channels was initially intended for the radio frequency interference (RFI) pixel identification. The AMSR2 features improved calibration with respect to AMSR-E and a higher spatial resolution due to larger antenna diameter. For AMSR2, the footprint size at 6.9 GHz is 35km by 62 km.

At 6.9 and 10.7 GHz, previous studies have shown that the scattering effects resulting from rain particles is usually smaller than 3 K, even in the presence of heavy rains [25]. The sensitivity to the ocean surface wind speed at horizontal polarization is larger than at vertical polarization [33]; at 6.9 GHz the sensitivity is about 1 K / (m/s) for wind speeds up to about 20 m/s [22].

2.2 Airborne stepped-frequency microwave radiometer measurements

The National Oceanic Atmospheric Administration (NOAA) Hurricane Research Division's (HRD) airborne SFMR onboard the NOAA WP-3D aircraft is the prototype for a new generation of operational airborne remote sensing instruments designed for the purpose of measuring the surface winds and rainfall in hurricanes. The SFMR observes the hurricanes at frequencies from 4.6 to 7.2 GHz, and provides along-track wind measurements up to 60 m/s [34]. Note that the observed SST and sea surface salinity used in the surface wind retrieval of SFMR are also provided by HRD. Its temporal and spatial resolutions are 1 s and ~1.5 km, respectively. The first experimental SFMR surface wind measurements were made during Hurricane Allen in 1980 [35], and the first operational transmissions of the SFMR winds to the Tropical Prediction Center/National Hurricane

Center (TPC/NHC) took place during Hurricane Dennis in 1999 [34]. The SFMR surface wind speed estimates have been validated against global positioning system (GPS) dropwindsonde measurements [36], and the root-mean-square error (RMSE) is approximately 4 m/s [37]. The SFMR-derived wind speeds in hurricanes were also validated against those retrieved using cross-polarized SAR data, with a bias and RMSE of -0.89 m/s and 3.24 m/s [15]. Recently, the SFMR tropical cyclone surface winds in heavy precipitation were further improved by using the new relationship between microwave absorption and rain rate [38], surface wind retrieval bias is significantly reduced in the presence of rain at wind speeds weaker than hurricane force.

In this study, the data from 53 hurricanes observed by the AMSR-E and AMSR2 between 2002 and 2014 are collected and collocated with the SFMR-measured wind speeds. Since the SFMR data could not provide the SST measurements before 2010, the HYCOM model-simulated SST has been included as an alternative for the matchup for storms before 2010. The spatial and temporal windows for collocation are 15 km and 15 minutes, respectively. The collocated dataset is used to develop and assess the high wind speed retrieval algorithm.

3. Method

3.1 Brightness temperature simulation with SSA/SPM model

The SSA/SPM are often used to simulate the ocean surface polarimetric thermal emissions [39-44]. By combining the emission contribution in the SPM from the standard incoherent Bragg scattering and the second order correction to the flat surface coherent reflection coefficient, one can write the surface brightness temperature as a function of the SST, Fresnel reflection coefficients, and surface directional wave spectrum [45] as follows:

$$T_{Bp} = T_s\left[(1-\left|R_{pp}^{(0)}\right|^2 - \int_0^{\infty} dk\, k \cdot \int_0^{2\pi} d\phi W(k,\phi) g_{pp}\right] \tag{1}$$

where, the subscript "*pp*" denotes the polarization (H or V for horizontal or vertical); T_{Bp} is the H- or V-polarized brightness temperatures; T_s is the sea surface temperature (SST); R_{pp} is the HH- or VV-polarized Fresnel reflection coefficients; k denotes the surface wave wavenumber; ϕ is the wave propagation angle with respect to the wind directions; $W(k,\phi)$ is the two dimensional (2D) wave elevation spectrum; and g_{pp} is the weighting function. The weighting functions at the HH and VV can be given as follows:

$$g_{HH} = 2\,\mathrm{Re}\{R_{HH}^{(0)*} f_{HH}^{(2)}\} + \frac{k_{zi}}{k_z}\left[\left|f_{HH}^{(1)}\right|^2 + \left|f_{HV}^{(1)}\right|^2\right]F \tag{2}$$

$$g_{VV} = 2\,\mathrm{Re}\{R_{VV}^{(0)*} f_{VV}^{(2)}\} + \frac{k_{zi}}{k_z}\left[\left|f_{VV}^{(1)}\right|^2 + \left|f_{VH}^{(1)}\right|^2\right]F \tag{3}$$

where, $k_0 = 2\pi/\lambda$, λ is the electromagnetic wavelength, $k_{zi} = k_0 \cos\theta_i$, $k_z = \sqrt{k_0^2 - k_x^2 - k_y^2}$, $k_x = k_{xi} + k\cos\phi$, $k_y = k_{yi} + k\sin\phi$, $k_{xi} = k_0 \sin\theta_i \cos\phi_i$ and $k_{yi} = k_0 \sin\theta_i \sin\phi_i$, and θ_i is the zenith angle of the incident direction. Re represents the real part operator, and * denotes the complex conjugate operation. $f_{\alpha\beta}^{(1)}$ and $f_{\alpha\beta}^{(2)}$ are the first and second order SPM scattering coefficients given in [39]. The first and second items on the right hand side of Equations (2) and (3) denote the second order coherent reflection contributions and the incoherent Bragg scattering contributions. The Function F in Equations (2) and (3) is defined to be 1 for k_z real, and 0 for k_z complex, and limits the incoherent contributions to waves propagating in the upper hemisphere [45].

The Fresnel reflection coefficients at the horizontal and vertical polarizations can be estimated using the following formulas:

$$R_{HH} = \frac{\cos\theta - \sqrt{\varepsilon - \sin^2\theta}}{\cos\theta + \sqrt{\varepsilon - \sin^2\theta}} \tag{4}$$

$$R_{VV} = \frac{\varepsilon\cos\theta - \sqrt{\varepsilon - \sin^2\theta}}{\varepsilon\cos\theta + \sqrt{\varepsilon - \sin^2\theta}} \tag{5}$$

where, θ is the incidence angle, ε is the relative permittivity of the seawater. The incidence angles of the AMSR-E and AMSR2 are both equal to 55° for all of the channels, with the exception of two channels at the 89 GHz. In this study, only the low frequency (6.9 GHz) T_B is used to develop the high wind speed retrieval algorithm.

3.2 High sea state surface roughness spectrum model

As the wind blows over the sea surfaces, it generates short-scale waves whose wavelengths are comparable to the incident electromagnetic (EM) waves. The ocean surface emissions are modified through the resonance interaction of these waves with the EM wave, and the changes of the local incidence angles from the tilting effects of the small-scale roughness by longer waves. For the purpose of simulating the normalized radar cross section under low and moderate sea states, a dimensionless surface roughness spectrum is empirically parameterized as a power-law function of the dimensionless wind speed (hereafter referred to as the H11 spectrum) [31]

$$B\left(\frac{u_*}{c};k\right) = A(k)\left(\frac{u_*}{c}\right)^{a(k)} \tag{6}$$

where, u_* is the wind friction velocity, c and k are the phase speed and wave number of the surface roughness wave component, they are related by the wave dispersion relation

$c=\sqrt{gk^{-1}+\tau k}$ in deep water; g is the gravitational acceleration, and τ is the ratio of surface tension and water density; $A(k)$ and $a(k)$ are the coefficients varying with the wavenumber k, which can be described using the analytical functions for the three branches covering difference wavenumber ranges [46]. The H11 spectrum worked well for $u_*/c<3$, (approximately $U_{10}<13\sim16$ m/s for Ku- and C-band, and $U_{10}<30$ m/s for L-band). For high wind speeds when the u_*/c is greater than 3, the wind speed exponent in the similarity property (6) becomes independent of the wavenumber. Accounting for this variation, the H11 spectrum was modified for high wind speeds (referred to as the H13 spectrum [32]), which has the following expression for $u_*/c\geq 3$:

$$B_h\left(\frac{u_*}{c};k\right)=A_h\left(\frac{u_*}{c}\right)^{a_h} \tag{7}$$

$$a_h=0.75 \tag{8}$$

$$A_h=A_{11}(k_m)(3)^{a_{11}(k_m)-0.75} \tag{9}$$

where, subscript h indicates the quantities for $u_*/c\geq 3$, and the two coefficients $A_{11}(k_m)$ and $a_{11}(k_m)$ are estimated with the H11 spectrum for the matching wavenumber k_m at $(u_*/c)_m=3$.

The ocean surface roughness spectrum B, and the 2D wave elevation spectrum W are related by:

$$B(u_*/c;k)=k^3\int_0^{2\pi}W(k,\phi)kd\phi \tag{10}$$

Therefore, Equation (1) can be rewritten as:

$$T_{Bp}=T_s\left(1-\left|R_{pp}^{(0)}\right|^2-\int_0^{\infty}B(u_*/c;k)k^{-3}g_{pp}dk\right) \tag{11}$$

where, the wind speed and wind friction velocity is connected by a drag coefficient (C_{10}): $u_* = U_{10}\sqrt{C_{10}}$. In this study, C_{10} is calculated using the empirical formula proposed in [31]: $C_{10} = 10^{-5}(-0.16U_{10}^2 + 9.67U_{10} + 80.58)$, which results in the computed wind friction velocity u_* increasing monotonically with U_{10} up to 50 m/s, and then decreasing for $U_{10} > 50$ m/s.

Under moderate sea states, the relative permittivity of sea water ε is a function of frequency, SST, and salinity. For high winds, the breaking waves bring air into the water column, and can lead to a drastic change of the relative permittivity of the resulting mixture ε_f . Using the equivalent medium approach, ε_f is computed with the seawater relative permittivity ε and the parameterized relationship between the whitecap coverage f_a , and the wind friction velocity [44]. Therefore, even for high wind speeds, the Fresnel reflection coefficients at the horizontal and vertical polarizations can be calculated with ε_f and incidence angle via Equations (4) and (5). The estimated Fresnel reflection coefficients are further used to compute the weighting functions according to Equations (2) and (3).

According to Equation (11), the T_B under moderate and high sea states can be simulated with SST, the Fresnel reflection coefficients, and the H13 spectrum for all wind speeds, which generates the H11 roughness spectrum at lower wind speeds. The wind speeds can be retrieved with this equation, by performing a nonlinear optimization that minimizes the difference between the SSA/SPM model-simulated T_B, and those measured by the AMSR-E and AMSR2.

4. Results and discussion

4.1 T_B simulations and comparisons

In this study, the AMSR-E and AMSR2 T_B observations have been collected at 6.9 GHz horizontal polarization overpass of 53 hurricanes between 2002 and 2014. They are then matched up with the SFMR-measured wind speeds, SST used for SFMR wind retrieval, as well as the HYCOM model-simulated SST. The collocated dataset is used to simulate the T_B with Equation (11), and then compared with those observed by the AMSR-E and AMSR2. For the purpose of brightness temperature comparisons and wind speeds validations, we make an average on SFMR along-track winds every 20 sample points before collocation to match the spatial resolutions of radiometers and SFMR. This operation enable us to obtain the SFMR winds with spatial resolution of 30 km. Moreover, for the comparisons, we used only those SFMR data which were acquired within 15 minutes difference from AMSR-E and AMSR2 acquisition. First, the SFMR wind speeds are used to estimate the ocean surface roughness spectrum using H11 and H13 spectrum models. Subsequently, the Fresnel reflection coefficients at horizontal and vertical polarizations are computed with the relative permittivity of air-water mixture ε_f, and the incidence angle. Finally, the SST from the SFMR surface wind retrieval or the HYCOM outputs, along with the estimated ocean surface roughness spectrum and the Fresnel reflection coefficients, are used to simulate the T_B at 6.9 GHz horizontal polarization channel.

As a case study, the T_B is simulated using the different ocean surface roughness spectrum (H11 and H13), and compared with the AMSR-E and AMSR2 observations over two typical hurricanes. Fig.1 shows that the modified ocean surface roughness spectrum, H13, achieved smaller bias and RMSE, either for Hurricane Earl (2010) or Edouard (2014). These statistics are documented in the figure legends, for example, the bias and RMSE for Hurricane Edouard are -0.21 K and 5.39 K, respectively, using the H13 spectrum. In addition to the T_B comparison for the case study, the statistical analysis and comparison of the entire collocated dataset is made. Figs. 2(a) and 2(b) show that the RMSE is 9.51 K for using the H11 spectrum, and 8.03 K for using the H13 spectrum. It is observed that when the T_B is smaller than 110 K, there is no significant difference between the T_B simulations using the H11 and H13 spectrum. However, when the T_B is larger than 110 K, the H11-derived T_B is less accurate than that calculated by using the H13 spectrum: the H11-derived T_B are overestimated in comparison to the AMSR-E and AMSR2 observations. This result suggests that the modified ocean surface roughness spectrum, H13, improved upon the T_B simulations to a certain extent, particularly for the high wind conditions. However, there is a tendency of underestimating T_B by using the H13 roughness spectrum. This will be further discussed in section 4.3.

4.2 Wind speed retrieval and validation

According to the SSA/SPM model, the T_B is related to the SST, Fresnel reflection coefficient, and ocean surface roughness spectrum (11). Therefore, the wind speed can be retrieved by performing a nonlinear optimization that minimized the difference between the measured and simulated T_B.

Figures 3(a), 3(b) and 3(c) illustrate the observed AMSR-E 6.9 GHz horizontal polarization T_B observations in Hurricane Earl (2010) over three continuous days (29-31 August 2010). These figures are used to study the evolution of the hurricane structure.

White pixels in Fig. 3 correspond to the land contaminated pixels in coastal areas as well as the RFI-contaminated areas. The exclusion of land contaminated pixels uses the global digital land topography and ocean bathymetry data ETOPO1 (http://www.ngdc.noaa.gov/mgg/global/global.html). Figs. 4(a), 4(b) and 4(c) show the AMSR-E Hurricane Earl rain rates from the Remote Sensing Systems (http://www.remss.com/missions/amsre). The rain bands in Fig. 4 match well with the T_B images in Fig. 3 for areas outside of the eyewall. In the hurricane eyewall regions, however, the spatial distribution patterns of AMSR-E rain rates and the T_B data show some discrepancies.

Figures 5(a), 5(b), and 5(c) illustrate the retrieved wind speeds using the SSA/SPM model and the H13 spectrum. The sequence of figures clearly illustrates the intensification process of Hurricane Earl. The retrieved wind speed pattern is very similar to the T_B observations (Fig. 3) that show clearly the hurricane structure. The maximum wind speed for the maximum level of the H13 spectrum is 51 m/s, and the spectrum becomes saturated as the wind speed exceeded this threshold. The black solid lines in Figs. 5(a) and 5(b) represents the SFMR tracks. The along-track SFMR wind speeds are used for validating the AMSR-E wind speed retrievals. Figs. 6(a), 6(b), and 6(c) illustrate the AMSR2 observed 6.9 GHz horizontal polarization T_B in Hurricane Edouard (2014) over three continuous days (15-17 September 2014). The AMSR2 rain rates are illustrated in Fig. 7. Again, rain rates and T_B observations exhibit similar and differential patterns outside and inside the hurricane eyewall. The AMSR2-retrieved wind speeds are shown in Fig. 8, in which the weakening process of Hurricane Edouard during these three days is clearly illustrated.

The AMSR2-retrieved wind speeds of the Hurricane Edouard on 16 September 2014 are compared with the collocated SFMR along-track measurements (Fig. 9). As illustrated, during the SFMR acquisition time (17:13~17:45 UTC), the AMSR2-retrieved winds along the track are in good agreement with the SFMR reference, except those occasions associated with heavy rain; the rain rate is also superimposed in Fig. 9. At the maximum rain rate of 24.9 mm/h, the corresponding wind speed bias is 7.8 m/s between AMSR2 retrieval (36.5 m/s) and SFMR measurement (44.3 m/s). For the two hurricanes used in the case study, the quantitative wind speed comparisons between the SFMR measurements and the AMSR-E and AMSR2 retrievals are shown in Figs. 10(a) and 10(b), respectively. The bias and RMSE are 1.08 and 3.93 m/s for Hurricane Earl, and 0.09 and 3.23 m/s for Hurricane Edouard. Along with the specific case studies, a statistical comparison is also conducted for the entire dataset consisting of 7080 matchup pairs. These pairs include the AMSR-E and AMSR2-observed horizontal polarization T_B acquired at 6.9 GHz channel over 51 hurricanes between 2002 and 2014, along with the SFMR measurements, or the HYCOM model-simulated SSTs when SSTs in the SFMR wind retrieval are not available. The statistical comparison results are shown in Fig. 11, with a bias of 1.11 m/s, and a RMSE of 4.34 m/s.

There are some factors that affected the AMSR-E and AMSR2 high wind speed retrievals. Examples of these factors included the SST, Fresnel reflection coefficient, ocean surface roughness spectrum, and rain effects. In this study, the SFMR data provide part of the SST inputs. However, there are time differences between the SFMR measurements and the AMSR-E and AMSR2 observations. Moreover, there are inherent errors that exist in the SSTs used in the SFMR wind retrieval. The Fresnel reflection coefficient estimation requires a good knowledge of the relative permittivity of the air-water mixture ε_f , but the whitecap parameter is difficult to calculate accurately under high wind conditions. Although the ocean surface roughness spectrum with high wind modification (H13 spectrum) shows distinct improvements in regards to the brightness temperature simulations, the upper bound of the roughness magnitude occurs at 51 m/s wind speed due to the relationship between u_* and U_{10} being non-monotonic, with u_* showing a maximum at U_{10} = 51 m/s.

4.3 Roughness spectrum

In this study, it is recognized that the calculated results of the microwave emissions and radar scattering from the ocean surfaces are critically influenced by the ocean surface roughness spectral model employed in the computation procedure. There have been many studies comparing the different spectral models [47-52]. See further discussion in section 2 of [32]. In this study, the H spectrum (H11 and H13) have been used. The H13 modifies the wind speed dependence in the high wind region ($u_*/c > 3$, corresponding to $U_{10} > 16$ m/s for the C-band). The modification is based on the observation, from analyzing the Ku-, C-, and L-band geophysical model functions (GMFs), that the wind speed sensitivity of the radar backscattering decreases in high winds. The sensitivity is expressed in terms of the wind speed exponent a in the similarity relationship of the ocean surface roughness (6): $B(k) = A(k)(u_*/c)^{a(k)}$. The H13 treats this sensitivity change as a simple two-branch transition, which seemed to be sufficient for the Ku- or L-band. However, it is somewhat too simplistic for the C-band. This has been found in the NRCS computations [53]. The T_B computations presented in this study further confirms that whereas the H11 overestimates the surface roughness, the H13 has over-corrected and yields a slight underestimation. We also tried the modification of the roughness spectrum (H15) presented in [53]. The results are not better than H13. Clearly, there is still plenty of area for improvement in the ocean surface roughness spectrum, particularly for the C-band. As a test run, the average of H11 and H13 (denoted as <H11, H13>) are used as the input roughness spectrum for computing the T_B and wind speed retrieval. This method produced a mixed result. The bias is improved but the RMSE is somewhat worse for the T_B ([-0.41, 8.24] K for <H11, H13> vs. [-1.89, 8.03] K for H13), whereas, the bias and RMSE statistics are somewhat better for the U_{10} ([0.22, 3.96] m/s for <H11, H13> vs. [1.11, 4.34] m/s for H13). The scatter plots for both the T_B and U_{10} are shown in Figs. 12(a) and 12(b), respectively. Based on this analysis, <H11, H13> is recommended for the operational application of wind retrieval using C-band microwave frequencies.

It is of interest to compare the relative magnitude of the two terms representing flat surface and roughness contributions, respectively, $e_0 = 1 - \left| R_{pp}^{(0)} \right|^2$ and $e_r = \int_0^\infty dk\, k \cdot \int_0^{2\pi} d\phi W(k,\phi) g_{pp}$ in Equation (1). Recent study presents the computation of the first term with consideration of the whitecap modification of the relative permittivity for Ku- and C-band frequencies [53]. For the θ=55° and wind speed up to 42 m/s, the range of e_0 is about 0.23~0.31 for C-band horizontal polarization. It should be noted that the first value is corresponding to flat surface, namely wind speed is 0 m/s, and the difference between the two numbers is the contribution of whitecap modification of the relative permittivity excluding the roughness contribution. That is, the whitecap modification is estimated to be 0~0.08 for C-band horizontal polarization.

The combined roughness and whitecap effects can be estimated from the radiometer data. Previous study reported a global dataset of WindSat microwave radiometer measurements with wind speed coverage up to about 42 m/s [29]. The WindSat measurements include five microwave frequencies (6, 10, 18, 23 and 37 GHz) for both vertical and horizontal polarizations, and the nominal incidence angle is 53°. These data are summarized in Fig. 5 of [53]. Using the nominal sea surface temperature T_s=290 K given by [29], the range of combined roughness and whitecap effect $\Delta e=\Delta T_B/T_s$ is about 0~0.11 for C-band horizontal polarization, corresponding to a brightness temperature range of about 32 K. In our study, the results (Fig. 2) show that the range of the C-band horizontal polarization combined ΔT_B is about 80 to 180 K based on the AMSR-E and AMSR2 data (Figs. 2, 12) with the wind speed range between 5 and 50 m/s (Fig. 11), that is, the range of brightness temperature spread is about 100 K. It is clarified here that the data of [29] are collected over many years and obviously averaged with an unknown but large degree of freedom. The range of AMSR-E and AMSR2 described above is not as heavily averaged and represent more localized or instantaneous values, therefore the wider range of the brightness temperature spread. A more extensive discussion of the various terms of roughness and whitecap contributions to the emissivity and their dependence on frequency, incidence angle and wind speed are given in [44].

4.4 Rain effects on wind retrieval

For the passive satellite radiometers operated at high frequencies, atmospheric absorption, emission and scattering associated with high level of cloud liquid water content and precipitation prevalent in hurricanes can have a large impact on T_B. Low frequency C-band channel (6.9 GHz) T_B are less sensitive to atmosphere and rain but are more sensitive to high winds than those from X- (10.7 GHz) and Ka-bands (36.5 GHz). Scattering can be neglected if the microwave wavelength is much larger than the raindrop size. Study showed that the rain scattering can be neglected for frequencies below 10 GHz up to 12 mm/h of rain rate [30], and the rain-induced scattering at 6.9 GHz might be negligible even in heavy rain condition [25]. The radiative absorption by rain needs to be taken into account for retrieving ocean surface winds under rain in severe weather conditions [38, 59].

Our SSA/SPM model described the relation between T_B and sea surface temperature, Fresnel reflection coefficient and ocean surface roughness spectrum under high wind conditions. This model can be used to simulate the dominant microwave emissions from the flat ocean surface and from wind-driven surface roughness and breaking-wave generated foam. According to [28], the excess emission associated with the wind-driven surface roughness and breaking-wave generated foam is on the order of 10 K, and up to 20 K in gale force winds. While the atmospheric emission is on the order of 5 K including reflected downwelling and upwelling. The wind and wave-induced excess emissivity at C-band (6.9 GHz) is about three times more sensitive to changes in sea surface roughness and foam than at L-band (1.4 GHz) in high wind conditions [28]. Thus, under hurricane wind conditions, the emission contributions from sea surface temperature, surface roughness and foam are far greater than those from atmospheric emission and absorption. Moreover, recent study also demonstrated that the contributions of ocean emissivity driven by winds are much larger than those from absorption by atmosphere [54].

The impact of precipitation on T_B is generally represented by an attenuation coefficient, which is a function of liquid water content, frequency, atmospheric temperature and pressure [55-56]. It is very difficult to accurately model brightness temperatures in rain. Because of the high variability of rainy atmospheres, the brightness temperatures depend on cloud type and the distribution rain within the footprint [57-58]. In addition, with increasing drop size, atmospheric scattering starts to become important. This means that it is impossible to use the simple Rayleigh approximation for cloud-water absorption [29], and it is necessary to apply the full Mie absorption theory. This requires additional information such as size and form of the rain drops. However, those parameters are not readily available. Under certain assumptions, for example, assuming that the hurricane structures are symmetry, the separation of the ocean radiation from the precipitating atmosphere can be implemented by using both C- and X-band channel T_B [59], but in general conditions, the hurricane structures are asymmetric. In a recent study [38], for the purpose of investigating the impact of rain on the measured microwave T_B on wind speeds weaker than hurricane-force, a new C-band relationship between microwave absorption and rain rate was developed, using aircraft Doppler radar reflectivity and simultaneous in situ Droplet Measurement Technologies Precipitation Imaging Probe (PIP) measurements. However, this empirical relationship cannot be directly used for estimating rain absorption effect on the AMSR2 or AMSR-E T_B.

It should be noted that the rain absorption effect on the T_B is not taken into account in our model. This effect can generally increases T_B under high rain rates and thus causes the wind speed overestimation. In this study, the wind speed bias is quantified over a broad range of radiometers-retrieved wind speeds and SFMR measurements. We find that the retrieved wind speeds are larger than SFMR measurements when the wind speeds are above 30 m/s, which are partly caused by the increasing brightness temperatures associated with the heavy rain. Fig. 13(a) shows the retrieval errors, whether the bias or the RMSE, increase with wind speeds. We estimate the effect of different rain rates on the wind speed retrieval accuracy as shown in Fig. 13(b). The general trend is that the wind speed retrieval errors increase with increasing rain rates, with a quasi-plateau region in the rain rate range between about 10 and 20 mm/h. Further studies are certainly needed to separate rain-induced T_B from the radiometer T_B observations under hurricane conditions, which has the potential to improve high wind speed retrieval accuracy particular in the hurricane eyewall regions.

5. Summary

In this study, a wind speed retrieval algorithm for the AMSR-E and AMSR2 hurricane observations has been developed. C-band (6.9 GHz) horizontal polarization T_B is used to measure high winds inside hurricanes, due to the fact that the T_B acquired at this frequency is sensitive to high wind speeds, and the rain scattering effects are weaker than other relatively higher frequency channels. Based on the SSA/SPM model, two different ocean surface roughness spectra (H11 and H13) are used to simulate the T_B, and then compare the simulations with the AMSR-E and AMSR-2 observations. The results show that the T_B estimated by the modified spectrum (H13) with high wind correction is closer to satellite measurements. Using the SST and estimated roughness spectrum, as well as the Fresnel reflection coefficients, the wind speeds are retrieved by performing a nonlinear optimization that minimized the difference between the measured and simulated T_B. Then, the retrieved wind speeds are compared with the corresponding SFMR measurements. The bias and RMSE are found to be 1.08 and 3.93 m/s for Hurricane Earl, and 0.09 and 3.23 m/s for Hurricane Edouard. The AMSR-E and AMSR2-derived wind speed patterns over three continuous days clearly show the intensifying and weakening processes, respectively, for Hurricane Earl and Edouard. The AMSR-E and AMSR2 6.9 GHz T_B are collected over 53 hurricanes between 2002 and 2014, which are collocated with the SFMR-measured wind speeds and resulted in 7839 wind speed matchup pairs. Using the 7080 pairs (excluding Hurricanes Earl and Edouard) from the collocated dataset, a statistical assessment on the wind speed retrieval is performed. The results show that the bias and RMSE of the retrieved wind speeds are 1.11 and 4.34 m/s. The wind speed retrieval accuracy is influenced by factors such as the SST, Fresnel reflection coefficients, ocean surface roughness spectrum and rain. The wind speed retrieval accuracy has potential to be improved by implementing a coupled wind-rain geophysical model function that can more accurately accounts for the microwave contribution from rain.

Acknowledgements

The authors would like to thank the National Snow and Ice Data Center (NSIDC), and the Japan Aerospace Exploration Agency (JAXA), who provided the AMSR-E and AMSR2 brightness temperature data. This research study was supported by National Science Foundation of China grant 41476158; Chinese National High Technology Research and Development (863) Program Grant 2013AA09A505; National Program on Global Change and Air-Sea Interaction Grant GASI-IPOVAI-04; NASA NNX14AM69G and the Office of Naval Research, Naval Research Laboratory publication number NRL/JA/7260-15-0186. The authors also thank the three anonymous reviewers for their constructive suggestions that greatly improve the manuscript. The views, opinions, and findings contained in this report are those of the authors, and should not be construed as official NOAA or US Government positions, policies, or decisions.

References

[1] S. H. Yueh, B. W. Stiles, and W. T. Liu, "QuikSCAT wind retrievals for tropical cyclones," *IEEE Trans. Geosci. Remote Sens.*, vol. 41, no. 11, pp. 2616-2628, 2003.

[2] B. A. Williams and D. G. Long, "Estimation of hurricane winds from SeaWinds at ultrahigh resolution," *IEEE Trans. Geosci. Remote Sens.*, vol. 46, no. 10, pp. 2924-2935, 2008.

[3] B. W. Stiles and R. S. Dunbar, "A neural network technique for improving the accuracy of scatterometer winds in rainy conditions," *IEEE Trans. Geosci. Remote Sens.*, vol. 48, no. 8, pp. 3114-3122, 2010.

[4] G.-J. van Zadelhoff, A. Stoffelen, P. W. Vachon, J. Wolfe, J. Horstmann, and M. Belmonte Rivas, "Scatterometer hurricane wind speed retrievals using cross polarization," *Atmos. Meas. Tech. Discuss.*, vol. 6, pp. 7945-7984, 2013.

[5] J. Horstmann, H. Schiller, J. Schulz-Stellenfleth, and S. Lehner, "Global wind speed retrieval from SAR," *IEEE Trans. Geosci. Remote Sens.*, vol. 41, pp. 2277-2286.

[6] X. Yang, X. Li, W. G. Pichel, and Z. Li, "Comparison of ocean surface winds from ENVISAT ASAR, MetOp ASCAT scatterometer, buoy measurements and NOGAPS

model," *IEEE Trans. Geosci. Remote Sens.*, vol. 49, pp. 4743-4750, doi:10.1109/TGRS.2011.2159802, 2011.

[7] B. Zhang, W. Perrie, P. W. Vachon, X. Li, W. G. Pichel, J. Guo, and Y. He, "Ocean vector winds retrieval from C-band fully polarimetric SAR measurements," *IEEE Trans. Geosci. Remote Sens.*, vol. 50, pp. 4252-4261, 2012.

[8] B. Zhang, X. Li, W. Perrie, and Y. He, "Synergistic measurements of ocean winds and waves from SAR," *J. Geophys. Res. Oceans.*, vol. 120, doi: 10.1002/2015JC011052, 2015.

[9] J. Horstmann, D. R. Thompson, F. Monaldo, S. Iris, and H. C. Graber, "Can synthetic aperture radars be used to estimate hurricane force winds?" *Geophys. Res. Lett.*, vol. 32, L22801, doi:10.1029/2005GL023992, 2005.

[10] H. Shen, W. Perrie, and Y. He, "A new hurricane wind retrieval algorithm for SAR images," *Geophys. Res. Lett.*, L21812, doi:10.1029/2006GL027087, 2006.

[11] H. Shen, Y. He, and W. Perrie, "Speed ambiguity in hurricane wind retrieval from SAR imagery," *Int. J. Remote Sens.*, vol. 30, pp. 2827-2836, 2009.

[12] A. Reppucci, S. Lehner, J. Schulz-Stellenfleth, and C. S. Yang, "Extreme wind conditions observed by satellite synthetic aperture radar in the North West Pacific," *Int. J. Remote Sens.*, vol. 29, pp. 6129-6144, 2008.

[13] A. Reppucci, S. Lehner, J. Schulz-Stellenfleth, and S. Brusch, "Tropical cyclone intensity estimated from wide-swath SAR images," *IEEE Trans. Geosci. Remote Sens.*, vol. 48, pp. 1639-1649, 2010.

[14] P. A. Hwang, B. Zhang, and W. Perrie, "Depolarized radar return for breaking wave measurements and hurricane wind retrieval," *Geophys*. *Res*. *Lett*., vol. 37, L01604, doi:10.1029/2009GL041780, 2010.

[15] B. Zhang, and W. Perrie, "Cross-polarized synthetic aperture radar: a new potential measurement technique for hurricanes," *Bull*. *Amer*. *Meteor*. *Soc*., vol. 93, pp. 531-541, 2012.

[16] B. Zhang, W. Perrie, Jun. A. Zhang, E. W. Uhlhorn, and Y. He, "High-resolution hurricane vector winds from C-band dual-polarization SAR observation," *J*. *Atmos*. *Oceanic Technol*., vol. 31, pp. 272-286, 2014.

[17] B. Zhang, W. Perrie, "Recent progress on high wind speed retrieval from multi-polarization SAR imagery: A review," *Int*. *J*. *Remote Sens*., vol. 35, pp. 4031-4045, 2014.

[18] G. Zhang, B. Zhang, W. Perrie, Q. Xu, "A hurricane tangential wind profile estimation method for C-band cross-polarization SAR," *IEEE Trans*. *Geosci*. *Remote Sens*., vol. 52, pp. 7186-7194, doi:10.1109/TGRS.2014.2308839, 2014.

[19] J. Horstmann, S. Falchetti, C. Wackermann, S. Maresca, M. J. Caruso, and H. C. Graber, "Tropical cyclone winds from C-band cross-polarized synthetic aperture radar," *IEEE Trans*. *Geosci*. *Remote Sens*., vol. 53, pp. 2887-2898, 2015.

[20] B. Zhang, W. Perrie, and Y. He, "Wind speed retrieval from RADARSAT-2 quad-polarization images using a new polarization ratio model," *J*. *Geophys*. *Res*., vol. 116, C08008, doi:10.1029/2010JC006522.

[21] P. W. Vachon, J. Wolfe, "C-band cross-polarization wind speed retrieval," *IEEE Geosci*. *Remote Sens*. *Lett*., vol. 8, pp. 456-459, 2011.

[22] A. Shibata, “A wind speed retrieval algorithm by combining 6 and 10 GHz data from advanced microwave scanning radiometer: wind speed inside hurricanes,” *J. Oceanogr.*, vol. 62, pp. 351-359, 2006.

[23] L. Meng, Y. He, J. Chen, and Y. Wu, “Neural network retrieval of ocean surface parameters from SSM/I data,” *Mon. Wea. Rev.*, vol. 135, pp. 586-597, 2007.

[24] F. Wentz, “Measurement of oceanic wind vector using satellite microwave radiometers,” *IEEE Trans. Geosci. Remote Sens.*, vol. 30, no. 5, pp. 960-972, 1992.

[25] B. Yan and F. Weng, “Applications of AMSR-E measurements for tropical cyclone predictions part I: retrieval of sea surface temperature and wind speed,” *Advances in Atmospheric Sciences*, vol. 25, no. 2, pp. 227-245, 2008.

[26] E. V. Zabolotskikh, L. M. Mitnik, and B. Chapron, “New approach for severe marine weather study using satellite passive microwave sensing,” *Geophys. Res. Lett.*, vol. 40, pp. 3347-3350, doi:10.1002/grl.50664, 2013.

[27] E. Zabolotskikh, L. Mitnik, and B. Chapron, “GCOM-W1 AMSR2 and MetOp-A ASCAT wind speeds for the extratropical cyclones over the North Atlantic,” *Remote Sens. Environ.*, vol. 147, pp. 89-98, 2014.

[28] N. Reul, J. Tenerelli, B. Chapron, D. Vandemark, Y. Quilfen, and Y. Kerr, “SMOS satellite L-band radiometer: A new capability for ocean surface remote sensing in hurricanes,” *J. Geophys. Res.*, vol .117, C02006, doi:10.1029/2011JC007474, 2012.

[29] T. Meissner, and F. J. Wentz, “Wind-vector retrievals under rain with passive satellite microwave radiometers,” *IEEE Trans. Geosci. Remote Sens.*, vol. 47, no. 9, pp. 3065-3083, 2009.

[30] F. T. Ulaby, R. K. Moore and A. K. Fung, “Microwave remote sensing III,” Artech House, 1986.

[31] P. A. Hwang, “A note on the ocean surface roughness spectrum”, *J. Atmos. Oceanic. Technol.*, vol. 28, pp. 436-443, 2011.

[32] P. A. Hwang, D. M. Burrage, D. W. Wang, and J. C. Wesson, “Ocean surface roughness spectrum in high wind conditions for microwave backscatter and emission computations,” *J. Atmos. Oceanic Technol.*, vol. 30, pp. 2168-2188, 2013.

[33] A. Shibata, “A change of microwave radiation from ocean surface induced by air-sea temperature difference,” *Radio Sci.*, vol. 38, pp. 8063-8072, 2003.

[34] E. W. Uhlhorn, and P. G. Black, “Verification of remotely sensed sea surface winds in hurricanes,” *J. Atmos. Oceanic Technol.*, vol. 20, pp. 99-116, 2003.

[35] W. L. Jones, P. G. Black, V. E. Delnore, and C. T. Swift, “Airborne microwave remote-sensing measurements of hurricane Allen,” *Science*, vol. 214, pp. 274-280, 1981.

[36] P. G. Black, E. W. Uhlhorn, M. D. Powell, and J. Carswell, “ cited 2011: A new era in hurricane reconnaissance: real time measurements of surface wind structure and intensity via microwave remote sensing,” [Available online at http://ams.confex.com/ams/last2000/techprogram/paper_12581.htm.]

[37] E. W. Uhlhorn, P. G. Black, J. L. Franklin, M. Goodberlet, J. Carswell, and A. S. Goldstein, “Hurricane surface wind measurements from an operational stepped frequency microwave radiometer,” *Mon. Wea. Rev.*, vol. 135, pp. 3070-3085, 2007.

[38] B. W. Klotz, and E. W. Uhlhorn, "Improved stepped frequency microwave radiometer tropical cyclone surface winds in heavy precipitation," *J*. *Atmos*. *Oceanic Technol*., vol. 31, pp. 2392-2408, 2014.

[39] S. H. Yueh, R. Kwok, F. K. Li, S. V. Nghiem, and W. J. Wilson, "Polarimetric passive remote sensing of ocean wind vectors," *Radio Sci*., vol. 29, no. 4, pp. 799-814, 1994.

[40] V. G. Irisov, "Small-slope expansion for thermal and reflected radiation from a rough surface," *Waves Random Media*., vol. 7, pp. 1-10, 1997.

[41] S. H. Yueh, "Modeling of wind direction signals in polarimetric sea surface brightness temperatures," *IEEE Trans*. *Geosci*. *Remote Sens*., vol. 35, no. 6, 1997.

[42] J. T. Johnson, and Y. Cai, "A theoretical study of sea surface up/down wind brightness temperature differences," *IEEE Trans*. *Geosci*. *Remote Sens*., vol. 40, no. 1, pp. 66-78, 2002.

[43] S. Guimbard, J. Gourrion, M. Portabella, A. Turiel, C. Gabarró, and J. Font, "SMOS semi-empirical ocean forward model adjustment," *IEEE Trans*. *Geosci*. *Remote Sens*., vol. 50, no. 5, pp. 1676-1687, 2012.

[44] P. A. Hwang, "Foam and roughness effects on passive microwave remote sensing of the ocean," *IEEE Trans*. *Geosci*. *Remote Sens*., vol. 50, no. 8, pp. 2978-2985, 2012.

[45] J. T. Johnson, M. Zhang, "Theoretical study of the small slope approximation for ocean polarimetric thermal emission," *IEEE Trans*. *Geosci*. *Remote Sens*., vol. 37, no. 5, pp. 2305-2316, 1999.

[46] P. A. Hwang, "Observations of swell influence on ocean surface roughness," *J*. *Geophys*. *Res*., vol. 113, C12024, doi:10.1029/2008JC005075, 2008.

[47] O. H. Shemdin, and P. A. Hwang, "Comparison of measured and predicted sea surface spectrum of short waves," *J. Geophys. Res.*, vol. 93, pp. 13883-13890, 1988.

[48] T. Elfouhaily, B. Chapron, K. Katsaros, and D. Vandemark, "A unified directional spectrum for long and short wind-driven waves," *J. Geophys. Res.*, vol. 102, pp. 15781-15796, 1997.

[49] R. Romeiser, W. Alpers, V. Wismann, "An improved composite surface model for radar backscattering cross section of the ocean surface: 1. Theory of the model and optimization/validation by scatterometer data," *J. Geophys. Res.*, vol. 102, pp. 25237-25250, 1997.

[50] W. J. Plant, "A stochastic, multiscale model of microwave backscatter from the ocean," *J. Geophys. Res.*, vol. 107, C93120, doi:10.1029/2001JC000909, 2002.

[51] P. A. Hwang, and W. J. Plant, "Analysis of the effects of swell and roughness spectra on microwave backsatter from the ocean," *J. Geophys. Res.*, vol. 115, doi:10.1029/2009JC005558, 2010.

[52] P. A. Hwang, D. M. Burrage, D. W. Wang, and J. C.C Wesson, "An advanced roughness spectrum for computing microwave L-band emissivity in sea surface salinity retrieval," *IEEE Geosci. Remote Sens. Lett.*, vol. 8, pp. 547-551, doi:10.1109/LGRS.2010.2091393.2011, 2011.

[53] P. A. Hwang, and F. Fois, "Surface roughness and breaking wave properties retrieved from polarimetric microwave radar backscattering," *J. Geophys. Res.*, vol. 120, pp. 3640-3657, doi:10.1029/2015JC010782, 2015.

[54] E. Zabolotskikh, L. Mitnik, and B. Chapron, “An updated geophysical model fro AMSR-E and SSMIS brightness temperature simulations over oceans,” *Remote Sens*., Vol. 6, pp. 2317-2342, doi: 10.3390/rs6032317, 2014.

[55] S. Matrosov, K. A. Clark, B. E. Martner, and A. Tokay, “X-band polarimetric radar measurements of rainfall,” *J*. *Appl*. *Meteor*., Vol. 41, pp. 941-952, doi:10.1175/1520-0450(2002)041<0941:XBPRMO>2.0.CO;2, 2002.

[56] S. Matrosov, D. E. Kingsmill, B. E. Martner, and F. M. Ralph, “The utility of X-band polarimetric radar for quantitative estimates of rainfall parameters,” *J*. *Hydrometeor*., Vol. 6, pp. 248-262, doi:10.1175/JHM424.1, 2005.

[57] F. J. Wentz and R. W. Spencer, “SSM/I rain retrievals within a unified all-weather ocean algorithm,” *J*. *Atmos*. *Sci*., Vol. 55, pp. 1613-1627, 1998.

[58] K. A. Hilburn and F. J. Wentz, “Intercalibrated passive microwave rain products from the unified microwave ocean retrieval algorithm (UMORA),” *J*. *Appl*. *Meteorol*. *Climatol*., Vol. 47, pp. 778-794, 2008.

[59] E. V. Zabolotskikh, L. M. Mitnik, N. Reul, and B. Chapron, “New possibilities for geophysical parameter retrievals opened by GCOM-W1 AMSR2,” *IEEE J*. *Sel*. *Topics Appl*. *Earth Observ*., Vol. 8, pp. 4248-4261, doi:10.1109/JSTARS.2015.2416514, 2015.

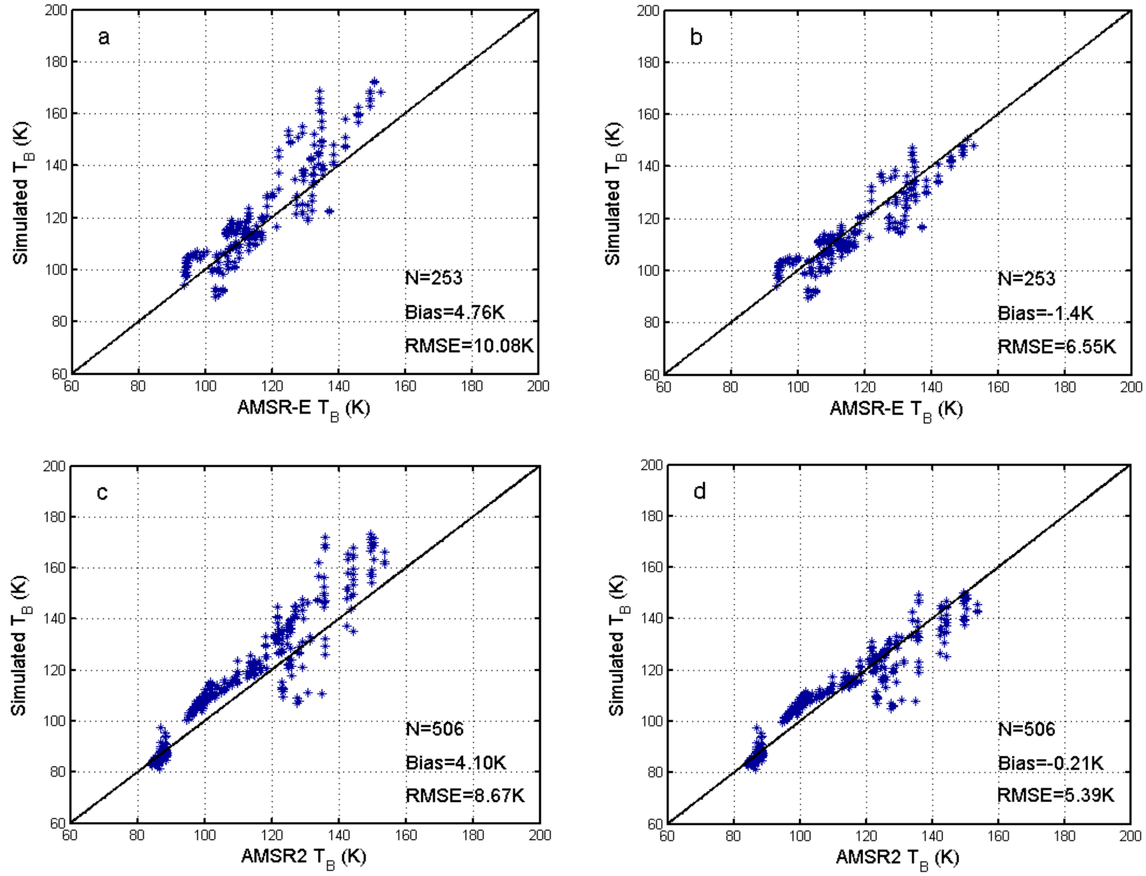

Fig. 1. Comparison between the AMSR-E and AMSR2 observed 6.9 GHz horizontal polarization brightness temperatures (T_B), and those simulated with the (a) H11 and (b) H13 spectrum for Hurricane Earl; and with the (c) H11 and (d) H13 spectrum for Hurricane Edouard.

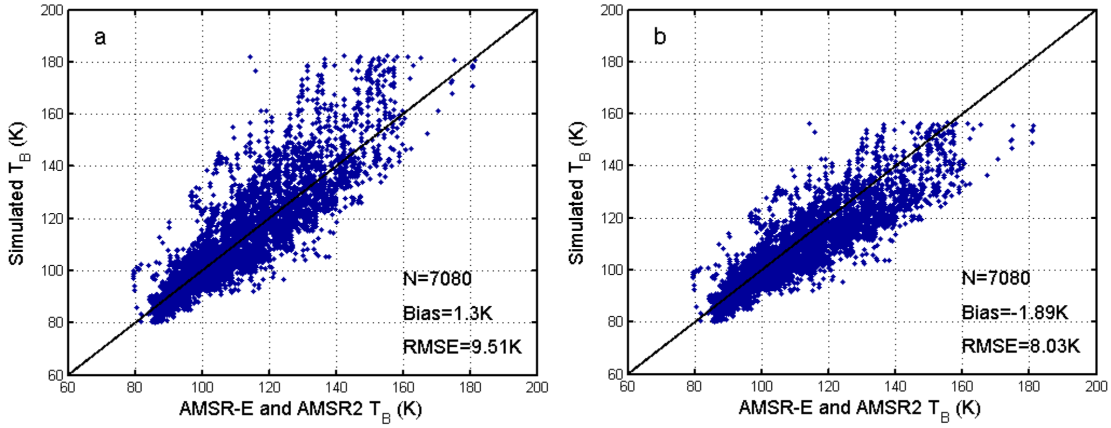

Fig. 2. Overall comparisons between the AMSR-E and AMSR2 observed 6.9 GHz horizontal polarization brightness temperatures (T_B), and those simulated with the (a) H11 spectrum (no high wind modification), and (b) H13 spectrum (high wind modification).

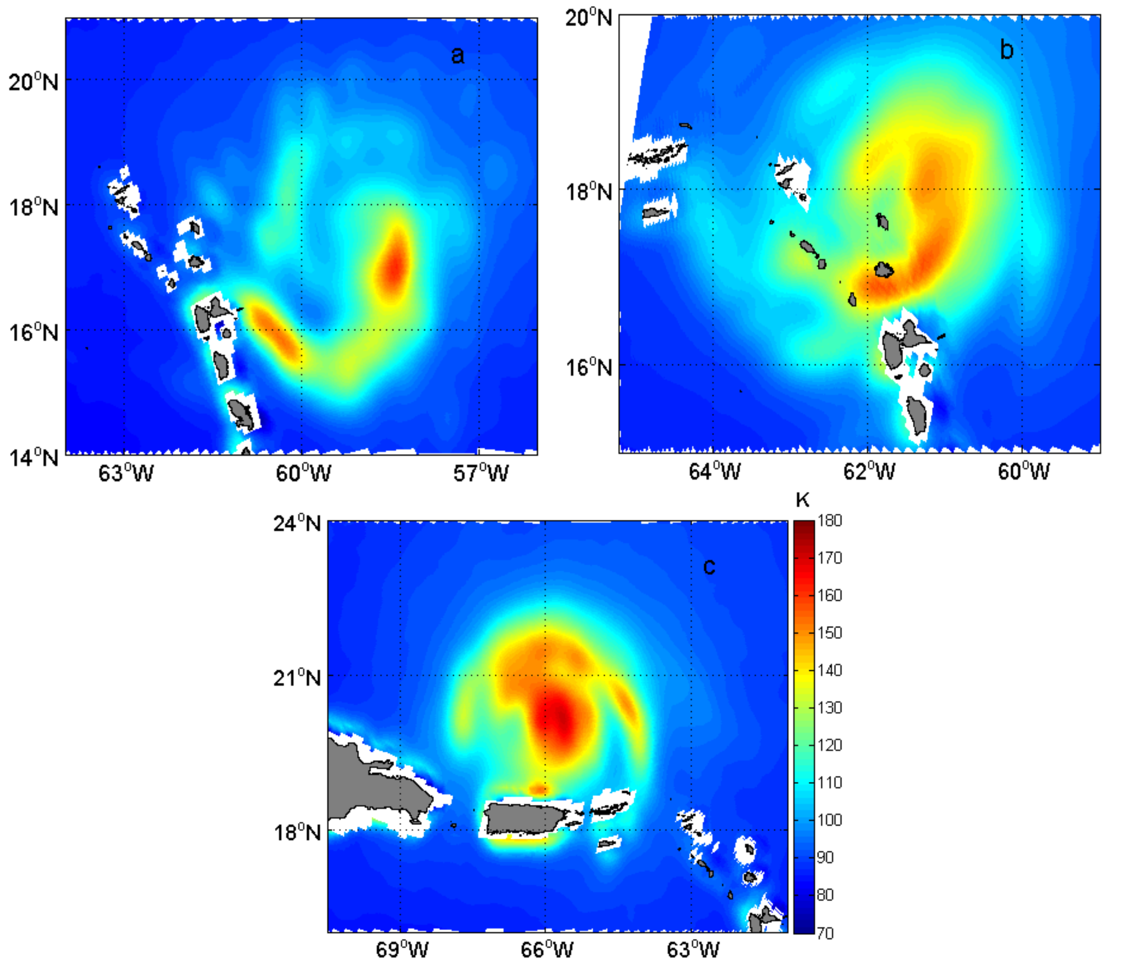

Fig. 3. AMSR-E observed 6.9 GHz horizontal polarization brightness temperatures (T_B) over Hurricane Earl on: (a) 29 August, 2010, at 1722 to 1726 UTC; (b) 30 August, 2010, at 0534 to 0537 UTC; and (c) 31 August, 2010, at 0615 to 0620 UTC.

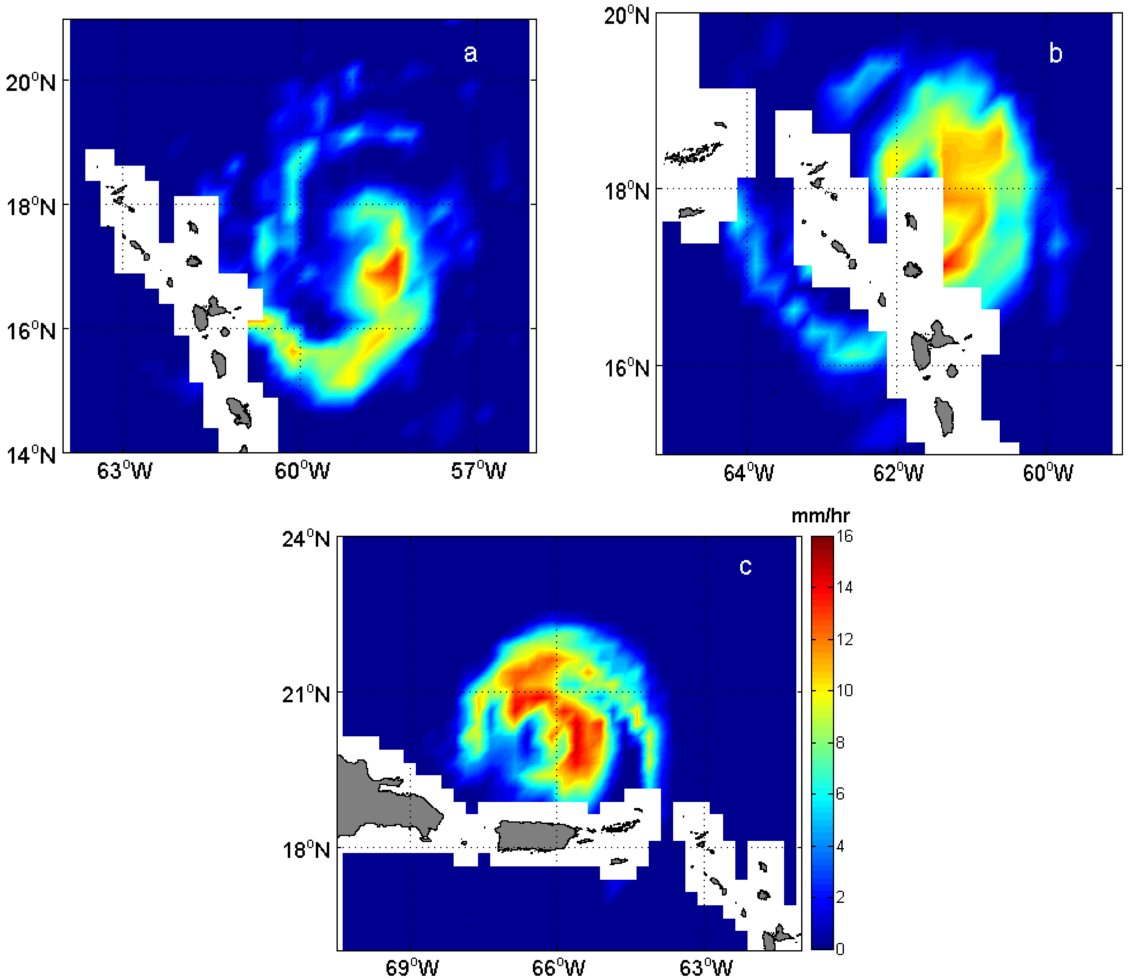

Fig. 4. The AMSR-E rain rates over Hurricane Earl on: (a) 29 August, 2010, at 1722 to 1726 UTC; (b) 30 August, 2010, at 0534 to 0537 UTC; and (c) 31 August, 2010, at 0615 to 0620 UTC.

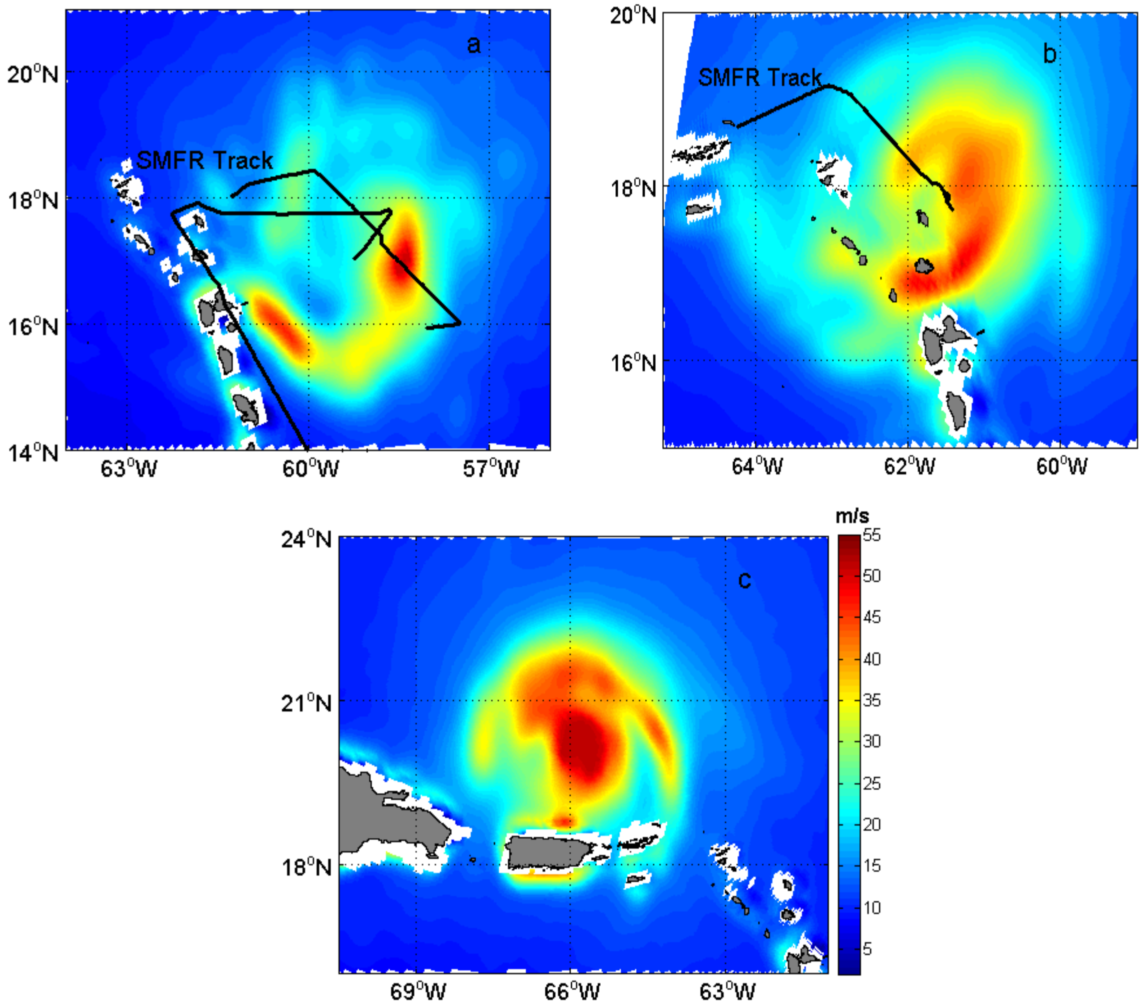

Fig. 5. Wind speed retrieval results from the SSA/SPM model and H13 spectrum, using the AMSR-E observed 6.9 GHz horizontal polarization brightness temperatures (T_B) over Hurricane Earl on: (a) 29 August, 2010, at 1722 to 1726 UTC; (c) 30 August, 2010, at 0534 to 0537 UTC; and (e) 31 August, 2010, at 0615 to 0620 UTC. The black solid lines in (a) and (b) represent the SFMR tracks, which were acquired on 29 August, 2010 at 1640 to 1750 UTC, and 30 August, 2010 at 0500 to 0600 UTC.

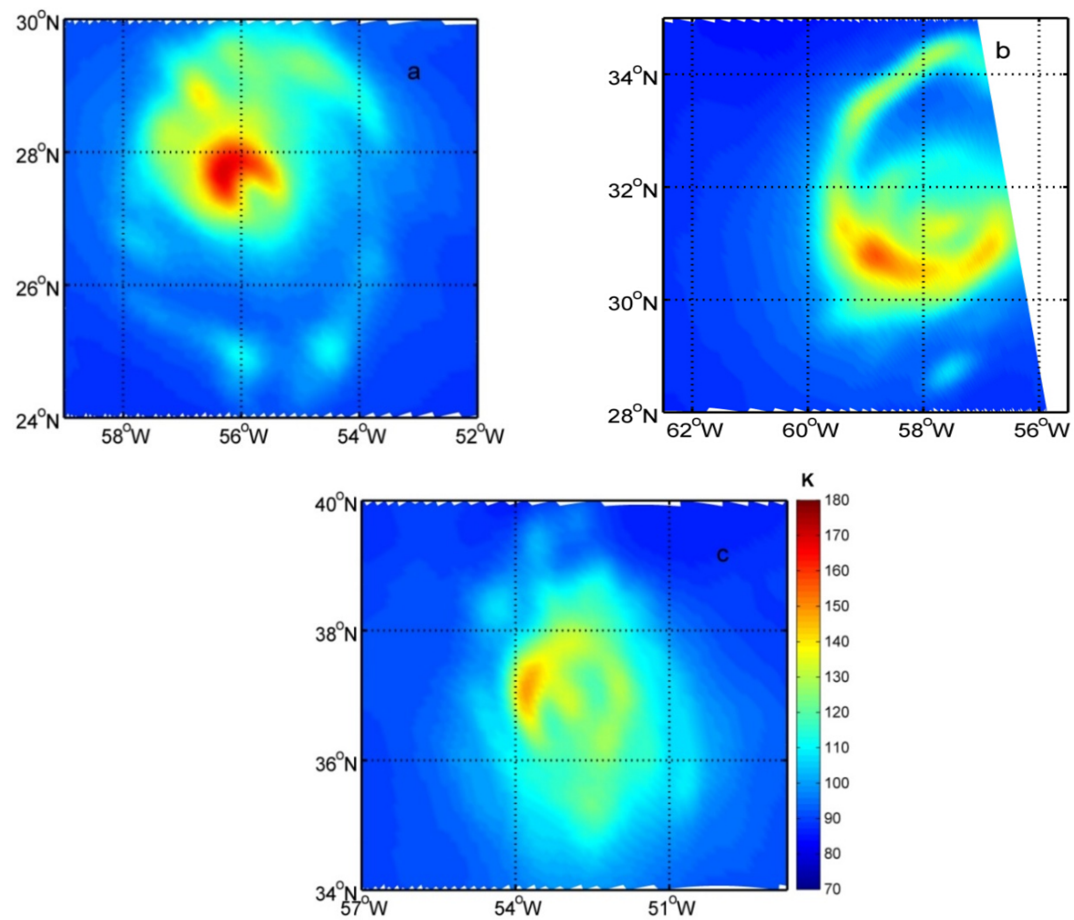

Fig. 6. AMSR2 observed 6.9 GHz horizontal polarization brightness temperatures (T_B) over Hurricane Edouard on: (a) 15 September, 2014, at 1645 to 1649 UTC; (b) 16 September, 2014, at 1729 to 1733 UTC; and (c) 17 September, 2014, at 1633 to 1637 UTC.

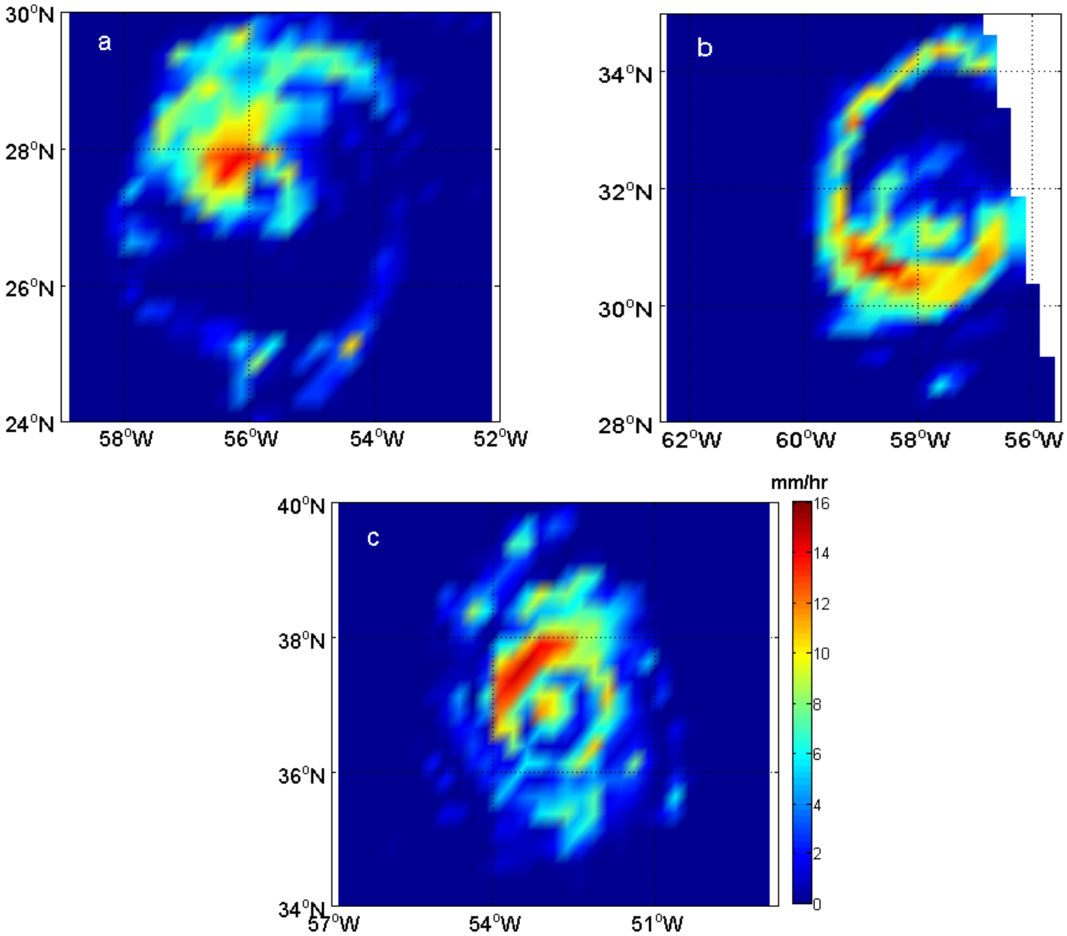

Fig. 7. The AMSR2 rain rates over Hurricane Edouard on: (a) 15 September 2014, at 1645 to 1649 UTC; (b) 16 September 2014, at 1729 to 1733 UTC; and (c) 17 September 2014, at 1633 to 1637 UTC.

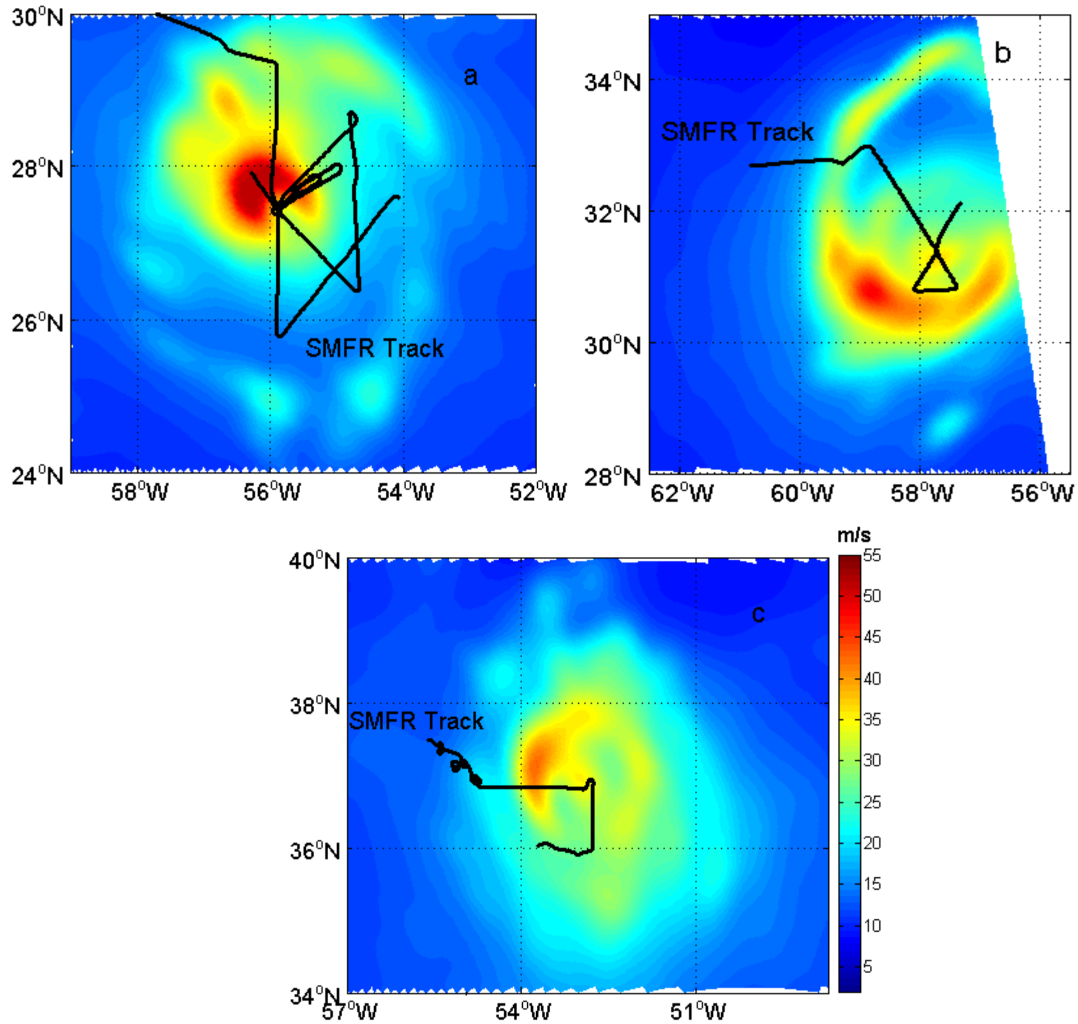

Fig. 8. Wind speed retrieval results from the SSA/SPM model and H13 spectrum, using the AMSR2 observed 6.9 GHz horizontal polarized brightness temperatures (T_B) over Hurricane Edouard on: (a) 15 September, 2014, at 1645 to 1649 UTC; (b) 16 September, 2014, at 1729 to 1733 UTC; and (c) 17 September, 2014, at 1633 to 1637 UTC. The black solid lines in (a), (b) and (c) represent the SFMR tracks, which were acquired on 15 September, 2014, at 1600 to 1510 UTC, 16 September, 2014 at 1650 to 1800 UTC, and 17 September, 2014, at 1600 to 1700 UTC.

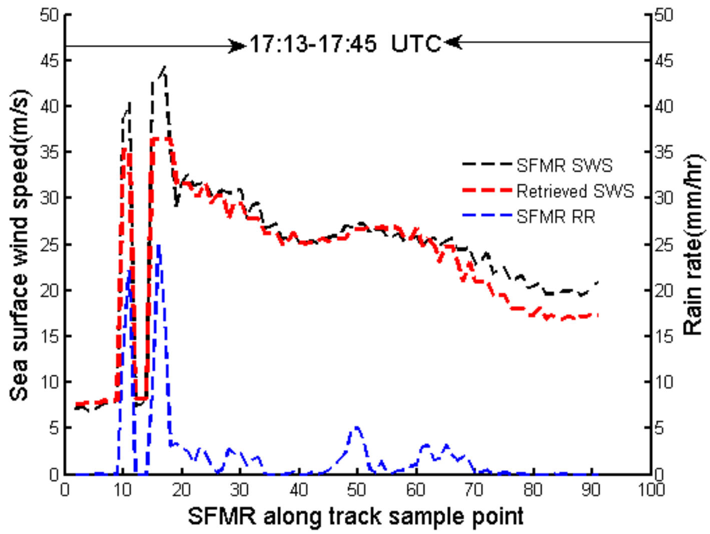

Fig. 9. AMSR2-retrieved SWS (red) and SFMR-measured SWS (black) in m/s and rain rate (RR) in mm/h for Hurricane Edouard as functions of sample points along the track on 16 September, 2014.

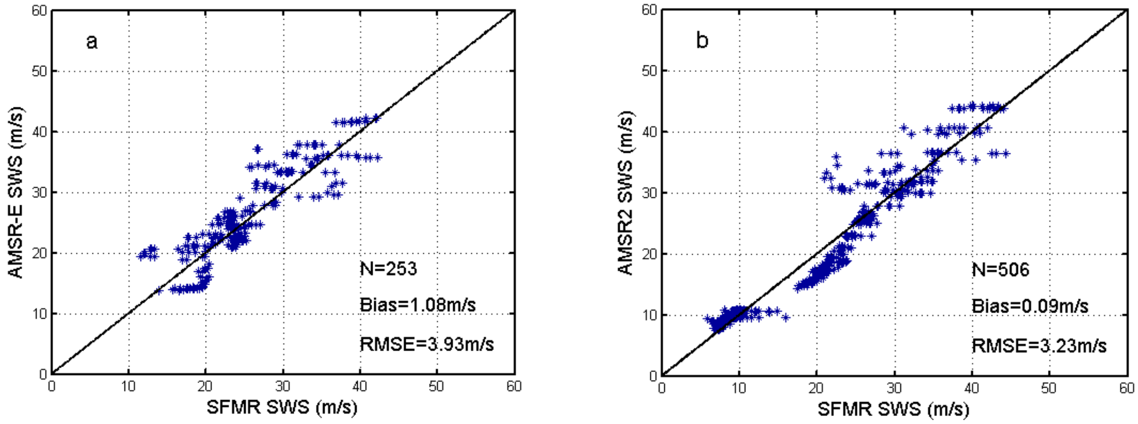

Fig. 10. SFMR wind speed measurements versus the AMSR-E and AMSR2 retrievals: (a) for Hurricane Earl; and (b) for Hurricane Edouard.

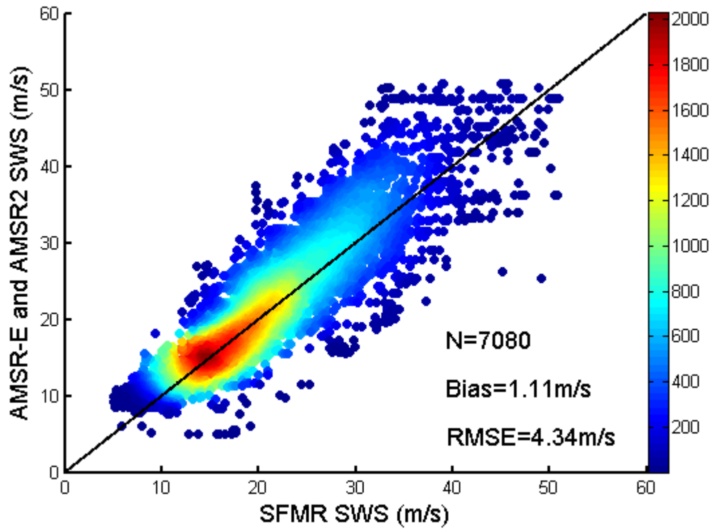

Fig. 11. SFMR wind speed measurements versus the AMSR-E and AMSR2 retrievals.

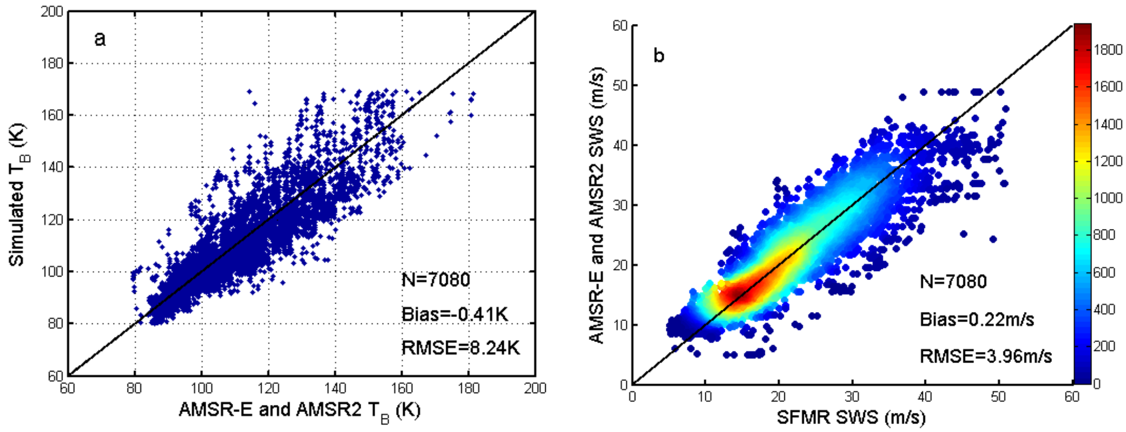

Fig. 12. (a) Overall comparisons between the AMSR-E and AMSR2 observed 6.9 GHz brightness temperatures (T_B), and those simulated with the averages of the H11 and H13 spectrum; and (b) SFMR wind speed measurements versus the AMSR-E and AMSR2 retrievals, using the averages of the H11 and H13 spectrum.

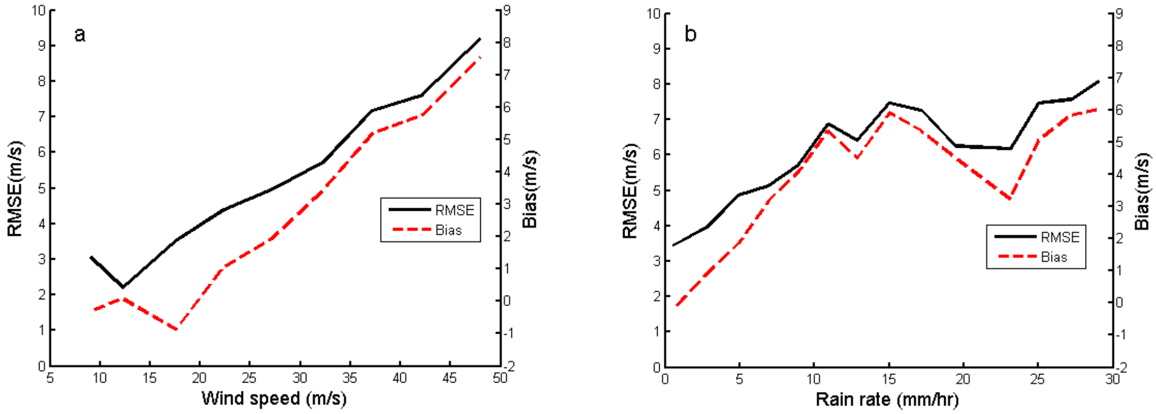

Fig. 13. The bias and RMSE of AMSR-E and AMSR2-retrieved wind speeds versus (a) wind speed, and (b) rain rate.